Improvement of the LPG-D probe with sensors and electronics for the objective assessment of burn scars in pediatric cases

Francesco Dalle Mura
Department of Industrial Technology
University of Florence
Florence, Italy
francesco.dallemura@unifi.it

Monica Carfagni
Department of Industrial Technology
University of Florence
Florence, Italy
monica.carfagni@unifi.it

Yary Volpe
Department of Industrial Technology
University of Florence
Florence, Italy
yary.volpe@unifi.it

2024 IEEE International Workshop on Metrology for Industry 4.0 & IoT (MetroInd4.0 & IoT) | 979-8-3503-8582-3/24/$31.00 ©2024 IEEE | DOI: 10.1109/MetroInd4.0IoT61288.2024.10584172

***Abstract*—Objective assessment of burn scars is critical for monitoring treatment efficacy and improving the quality of regenerated skin, particularly in pediatric cases where scar management is critical for long-term healing. In this context, this study presents an improvement with the introduction of sensors in the LPG-D (Louis Paul Guitay Device) probe, which was developed in the T3Ddy laboratory with the primary goal of objectively assessing burn scar pliability. The central component of the new prototipe is the incorporation of a magnetic encoder-based position detection system, which improves the accuracy and reliability of the pliability assessment. Through rigorous testing, including evaluation of maximum acquisition rate, repeatability of sensor measurements, and suction effect, the study demonstrated the device's ability to provide an accurate and reliable objective assessment of scar pliability. This advancement is very promising for improving the management of burn scar treatments in pediatric patients, enabling clinicians to make more informed decisions based on objective data. In addition, the study proposes a new software platform that integrates an angular encoder and a distance sensor, enabling simultaneous data reading and analysis. Taking advantage of the versatility and efficiency of the Python programming language, the software facilitates the interpretation of the device's position on the scar and its pliability, providing clinicians with useful information for treatment optimization.**

Keywords—Burn Scar, Objective evaluations, Distance sensor, LPG treatment.

I. Introduction

The healing process of the human body is a complex phenomenon involving several biological mechanisms aimed at repairing damaged tissue, with the primary goal of restoring tissue integrity [1]. However, this process can often lead to the formation of scars, which are the result of the body's natural response to injury. Scars can vary greatly in terms of aesthetic appearance and pathological impact, depending on several factors such as the depth and extent of the injury, as well as the individual characteristics of the patient [2].

Scar treatment is a process that often requires a multidisciplinary approach and may involve several therapeutic modalities, each aimed at mitigating the effects of scarring and improving the quality of the regenerated skin [3]. In case of burn scars, that is the subject of the present paper, the most common therapies include pressure therapy, the use of steroids, radiotherapy, laser treatments, massage and, in extreme cases, surgery. However, as each scar is unique, treatment must be customized according to the specific needs of the patient and the characteristics of the lesion [4], [5]

A thorough assessment of burn scars has a crucial role when determining the effectiveness of treatments and monitoring progress over time. Currently, in clinical practice, scar assessment is mainly based on subjective assessment scales, which involve visual observation and palpation by the physician. Examples of common assessment scales include the Vancouver Scar Scale, the Manchester Scar Scale and the Patient and Observer Scar Assessment Scale. However, these scales may be influenced by the subjectivity of the observer and may not provide a complete and objective assessment of scar characteristics [6], [7].

In recent years, there has been a growing interest in biomechanical skin assessment approaches that aim to provide a more objective and accurate assessment of scars [8], [9], [10]. Among the biomechanical properties of leather, pliability, i.e. its ability to deform, plays a key role in the evaluation of scars. However, scientific research has so far addressed the assessment of pliability in a limited manner, highlighting the need for further qualitative, objective, and reliable methods and measurement systems for this important parameter [11], [12], [13], [14].

To close this gap and create unbiased techniques for evaluating the health status of a burn scar in pediatric cases, a research project has been initiated within the T3Ddy lab a joint venture between Meyer Children's Hospital and the Department of Industrial Engineering at the University of Florence (Italy). In particular, the project focused on the assessment of pliability and developed a probe, called LPG-D, to objectively assess this parameter during LPG treatment sessions [15], [16]. The LPG treatment, which stands for Lipomassage, is a non-invasive procedure that uses a mechanical device to perform a deep tissue massage on both the skin and subcutaneous tissues. The aim of the treatment is to detach scarred areas and induce cells to produce collagen and elastin to restore the original skin properties. The LPG-D uses a distance sensor to quantify the lift of the scarred skin as the probe passes during treatment, allowing the doctor to monitor the change in pliability in real time as the treated area changes [17] (Fig. 1).

979-8-3503-8582-3/23/$31.00 ©2024 IEEE

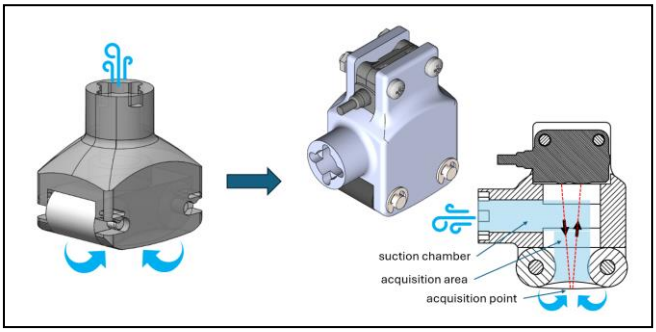

Fig. 1. On the right the LPG probe used for the Meyer massage, on the left the LPG-D probe. In the cross-sectional figure, it is possible to see the suction chamber (in blue), the acquisition zone (in red) and the acquisition point.

The sensor is aligned parallel to the probe support plane, using the principle of laser triangulation. It is positioned such that the acquisition point is exactly in the center of the suction zone. Several issues were discovered during the clinical usage of the LPG-D, one of which was the requirement for a more precise evaluation of pliability between subsequent therapy sessions to confirm the effectiveness of the therapies.

Therefore, based on these considerations and in agreement with Meyer's clinicians, this paper proposes an implementation of the LPG-D probe to provide an objective assessment of pliability by correlating distance sensor data with information on the position of the measured point. The device proposed in this study is made up of appropriately sized hardware that includes a system for correlating the position of the evaluated zone on the patient's scar in addition to an integrated LPG system with distance assessment sensors (similar to the LPG-D).

II. Materials and Methods

As previously mentioned, the new device integrates the LPG-D probe with a position measuring device and a microcontroller to correlate the sensor data and provide an output to the physician via software. Implementing a method to assess the point's location as measured by the probe was the first stage of the study. Next, appropriate hardware design and electronic component searches were conducted, and lastly, the new prototype was validated.

A. *Development of the position advancement evaluation system.*

In the preliminary phase of the design process, extensive analysis and planning were carried out to develop a system that would allow the precise evaluation of the movement of the probe over the scar during the treatment. The primary objective was to establish a close correlation between the position of the device and its measurements. It was determined that the evaluation of the rotation of one of the device's two rollers would be decisive in determining the advancement relative to the initial reference point. After some research, it was decided to use magnetic encoder-type sensors, which measure the rotation of a mechanical shaft by reading the magnetic field generated by a magnet [18] (Fig. 2).

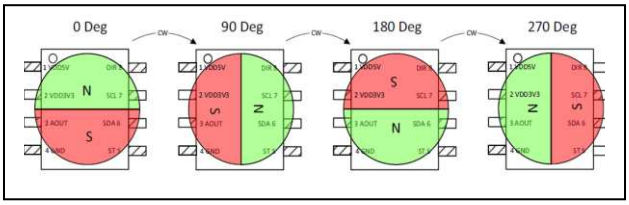

Fig 2. Diametral magnet with encoder sensor. Functional diagram rotation detection.

In order to transmit the rotation of the roller to the magnet placed in front of the sensor (encoder), a system has been developed whereby a small gear wheel, called the driving wheel, is used to transmit the motion of the roller to a larger wheel, called the leading wheel, inside which the magnet is placed. The sensor reads the angle of rotation, and the distance travelled is calculated using the pure rolling formula combined with the transmission ratio given by the toothed wheel (Fig. 3).

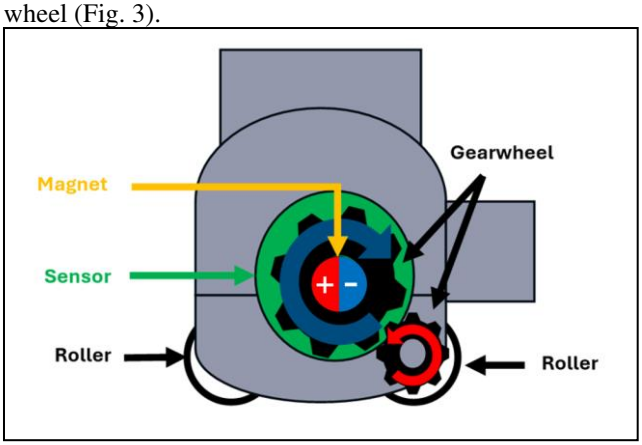

Fig. 3. Position advancement evaluation system diagram.

B. *Selection of components*

The components were selected with an emphasis on minimizing size and maximizing accuracy once the position detecting system was established to facilitate simple integration into the device without compromising its overall dimensions. The table below provides information on the selected components.

TABLE I. Description of the Components of the New Device.

Components	Commercial name	Dimensions	Description
Magnetic Angular Encoder	AS5600	17x15x2 mm	Accuracy of 12 bits when used with I2C interface or 10 bits when used via PWM readout [19]
Microcontroller	DFR0816-Beetle-CM of the DFRobot company	20.5x22x2 mm (excluding USB type-C port height)	Serial communication with the computer for programming via Arduino IDE [20].
Distance sensor	FT-10 RLA-60-PNSL-KM4 SensoPart	18.3x14.6x8 mm	Similar to the sensor in the LPG-D probe [21][1]. Measurement range[2]: 10-70 mm Resolution: 0.01 mm

[1] Reference material 5…90 % reflectivity.
[2] For more information on sensor technical data, refer to the datasheet cited.

Next, a circuit was developed to interconnect all the mentioned components. This circuit, together with the distance sensor, is connected to the PC via a USB port.

III. CAD DESIGN AND MODELLING

Using the 3D modelling software SOLIDWORKS®, an adaptation of the old device was carried out in order to allow the integration of the position detection system together with its components. Initially, the main body was slightly enlarged to allow the creation of dedicated housings: one for the microcontroller (µC) on the right-hand side and one for the sensor on the left-hand side. The body retains the same suction port as the original LPG machine, keeping the layout identical to the previous device. The model of the left carter was then produced together with the motion transmission system from the roller to the magnet (Fig. 4).

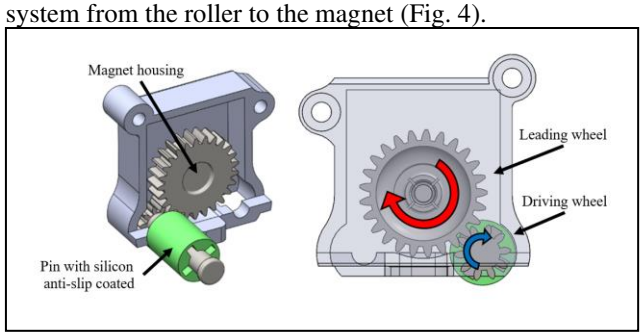

Fig. 4. Transmission block assembly consisting of the following elements: piece drive wheel with pin with silicon anti-slip coated, driven wheel, left housing. The movement diagram of the gearbox is shown on the right.

To place the magnet concentrically on the encoder, the following gear parameters were used: wheel modulus equal to 1.8, number of drive wheel teeth equal to 10, and number of driven wheel teeth equal to 25, resulting in a gear ratio of 2.5. This configuration makes it possible to keep the outer diameter of the drive wheel smaller than the outer diameter of the anti-skid silicone roller cover. This wheel is made as a single unit with the axle, which is equipped with fins that prevent relative rotation between the axle and the lining. The lining was made by casting silicone Dragon Skin 10 from the Smooth-On company [22] using a mold specially designed for this purpose. To provide a better understanding of the different components, Figure 5 displays both the exploded view of the assembly and the CAD model of the new prototype.

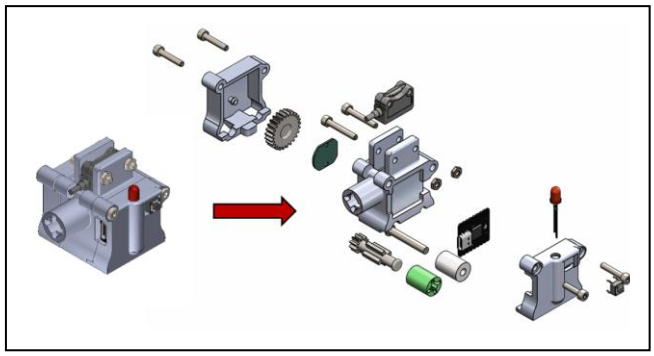

Fig. 5. On the left is the CAD model of the prototype of the new LPG-D probe. On the right is an illustration of the assembly.

From the exploded view, it is possible to observe the presence of two important components: an RGB LED intended to signal an error in the acquisition phase to the doctor, and a button whose purpose is to start and stop data acquisition. In particular, the light signal provides a clear indication if the maximum allowed speed is exceeded during sensor passage or if the roller does not roll correctly on the skin, thus preventing erroneous evaluations.

In order to produce the designed component, two distinct 3D printing methods were employed: stereolithography (SLA) for the carter and central body and fused deposition modeling (FDM) for all other components. The choice of SLA technology to produce the body was imposed by the constraint of reducing air leaks; in fact, with this technology, it is possible to produce a fully insulated part. The materials used are Grey Pro resin from Formlabs [23] for SLA and a PLA filament for FDM printer.

To further reduce the effects of leakage, miniskirts designed to completely cover the device's rollers were introduced (Fig. 6). By completely covering both the front and rear areas of the device with the miniskirts, there is a concentration of the suction effect in the central area, resulting in increased skin lift with the same suction force.

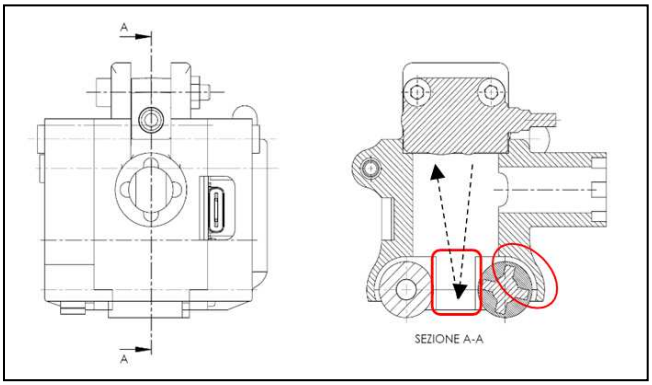

Fig. 6. The figure shows the front view of the device with the section line in the center. On the right, we see the section where the suction zone and roller cover are highlighted, and the dotted arrows indicate the laser path for distance measurement.

The sensitivity (S) of an encoder is defined as the angular displacement per encoder count and is crucial in assessing the device's resolution. Mathematically, the sensitivity is expressed by the formula:

$$S = \frac{2\pi}{2^n} \tag{1}$$

where:

- ***S*** denotes the sensitivity in radians per number of encoders.
- ***n*** denotes the number of bits in the encoder, which determines the resolution of the encoder.

As shown in the formula (1), encoder sensitivity is inversely proportional to the number of encoder bits (n). Consequently, increasing the number of bits reduces the sensitivity, indicating the ability to detect smaller position variations.

For example, given n = 10 bits, the sensitivity (S) of the encoder is calculated as follows:

$$S = \frac{2\pi}{2^{10}} = \frac{2\pi}{1024} \approx 0.006\, rad \tag{2}$$

This calculation gives the encoder sensitivity, which is approximately 0.006 radians per encoder count.

The sensitivity of the encoder is integrated into the overall sensitivity evaluation of the device, as represented by the formula.

$$X_s = \frac{D}{2} \cdot (Rt \cdot S) = \frac{11}{2}(2{,}5 \cdot 0{,}006) = 0{,}085 \text{ mm} \quad (3)$$

Here, *Xs* indicates the position variation perceived by the probe, *D* represents the driving gear diameter, *Rt* is the gear ratio, and S is the sensitivity of the encoder.

IV. Software Design

In conjunction with the hardware design phase, special software was developed to integrate the angular encoder and the distance sensor into a single software platform. The choice fell on the Python programming language in order to correlate the outputs of the two sensors. During the process, data from the AS5600 encoder (rotary angle sensor) is initially processed by the device's integrated microcontroller, configured via Arduino. Subsequently, this data is transmitted to the computer, where software written in Python acquires it simultaneously with the data coming from the distance sensor. This software made it possible to correlate the values acquired by the two sensors at the same time of acquisition, facilitating the analysis and interpretation of the data relating to the position of the device on the scar and its pliability.

This was completed with the implementation of a graphic interface to simplify the use of the device by the physician. The interface offers two distinctive functionalities to facilitate the management of acquired data during the treatment. Firstly, it manages data acquisition, allowing users to save them in a CSV file for further analysis. Additionally, if selected, the interface generates a graph corresponding to the acquired data, thus providing an immediate visual representation of the results.

The second functionality of the interface is equally significant, as it allows comparing data collected in two different treatment sessions. This comparison occurs by displaying the data in a single graph, enabling operators to assess the treatment's progress effectively and directly over time. This ability to directly compare treatment sessions represents a valuable tool for evaluating the overall effectiveness of the treatment and identifying any trends or improvements over time.

V. Tests and Results

In order to evaluate the prototype, three types of tests were carried out: the first is an evaluation test of the maximum acquisition speed; the second is an evaluation of the repeatability of the two sensors measurements; and finally, the last is an evaluation of the suction effect.

The first and second tests were conducted using an FDM-printed specimen characterized by 10-mm-wide steps, with depths varying between 1 and 9 mm in 0.1-mm increments, arranged randomly (Fig. 7).

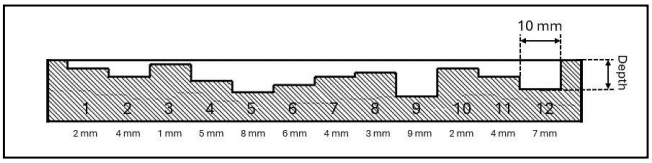

Fig. 7. Specimen made in FDM to test the repeatability of the new prototype. In the bottom part are reported the steps depth.

In the first case, the aim was to evaluate the limiting speed of the device sliding on the scar to have an acceptable pliability assessment. A linear guide was used to slide the device onto the specimen, progressively increasing the speed (Fig 8).

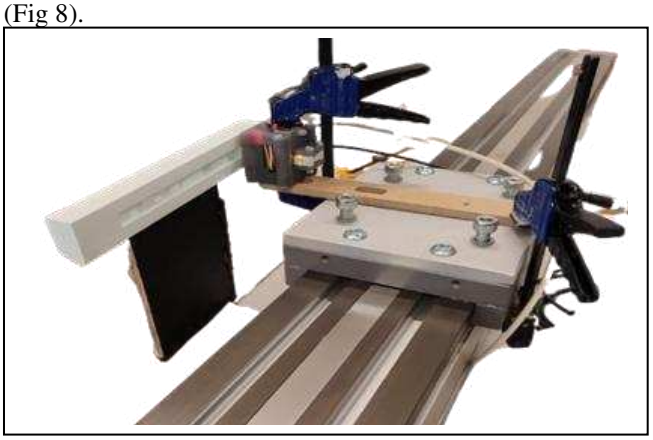

Fig. 8. Setup of the system to perform the maximum acquisition speed test.

By analyzing the software output values of the measured depth (shown in blue in Fig. 9) and combining them with the feed rate values (shown in red in Fig. 9), it was possible to identify the speed at which the measurement loses its significance due to the reduced number of points acquired.

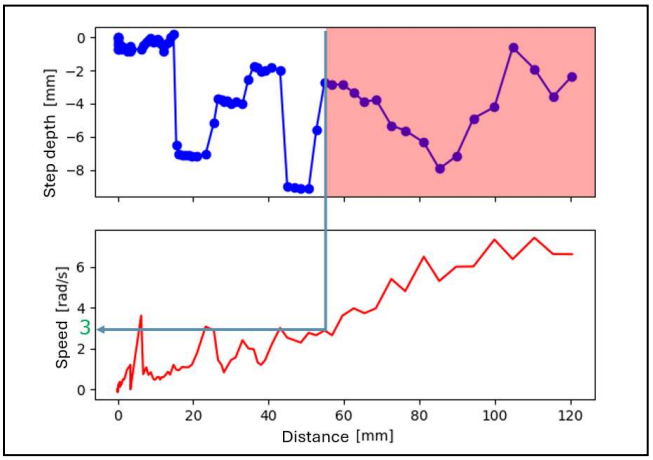

Fig. 9. In blue, the graph of the specimen step depths measured by the device as a function of distance is displayed. In red, the graph of the encoder rotation speed as a function of distance travelled is displayed.

The threshold speed value corresponds to 3 rad/s. This threshold value was set in the software design as a reference for switching the LED color from green to red, so that the doctor has visual feedback in real time.

The second test has two main objectives: to evaluate the repeatability of the measurement made by the distance sensor FT 10 RLA 60-PNSL and, at the same time, to measure the repeatability of the position detected by the encoder. The graph obtained from a single acquisition is shown in Fig. 10.

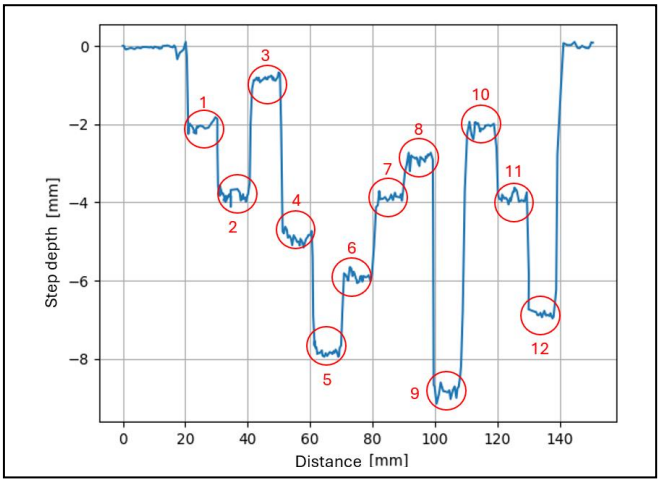

Fig. 10. graph of step depth as a function of the distance travelled by the probe. In red is shown the step number

Each step measurement consists of a series of point measurements performed by the sensor during its movement. Therefore, for each acquisition, the average of the point measurements was calculated and, subsequently, since several measurements of the specimen were taken, the average of the acquisitions for each corresponding step of the specimen. In addition, the standard deviation of the acquisitions was determined to assess the coherence of the measurements (Table II).

TABLE II. AVERAGE VALUE AND STANDARD DEVIATION ON THE MEASURAMENTS

Steps n°	Average value depth [mm]	Standard deviation [mm]
1	2,05	0,12
2	3,73	0,09
3	0,78	0,05
4	5,08	0,10
5	7,84	0,15
6	5,97	0,15
7	3,73	0,08
8	2,84	0,17
9	8,77	0,09
10	2,03	0,18
11	3,85	0,09
12	7,02	0,11

From the same data, it was possible to evaluate the repeatability of the measurement made with the encoder. In fact, it was possible to analyze the step widths obtained as the distance between two steps (the average position between the last point of one step and the first point of the adjacent step was taken as a reference) and compare it with the actual width of 10 mm (Fig. 11).

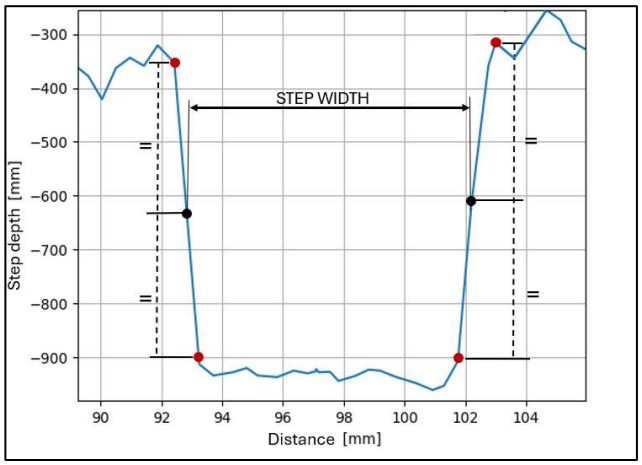

Fig. 11. Graph of step depth as a function of distance covered by the probe. Schematic diagram of the method for calculating step width. The first or last points of the step are highlighted in red, while the middle point between them is shown in black.

Using the width of all steps of all acquisitions as a sample we obtain a mean value of 9.93 mm with an absolute error of 0.5 mm and a standard deviation of 0.12 mm.

It should be noted that this error can be attributed to the presence of a sharp edge between one step and the next of the specimen, which interferes with the measurement of the depth sensor. However, it is important to emphasize that this problem does not occur in medical applications, as scars do not have sharp edges.

In the last test, to simulate suction on the skin, rectangular silicone pads (60 mm x 120 mm x 10 mm) with different Shore 00 hardnesses were used to simulate varying elasticity; in particular, the silicones Ecoflex 00.10, Ecoflex 00.30, and Ecoflex 00.50 from the company Smooth On were used [24]. The specimens were placed side by side and aligned by positioning them in descending order of hardness (Fig.12).

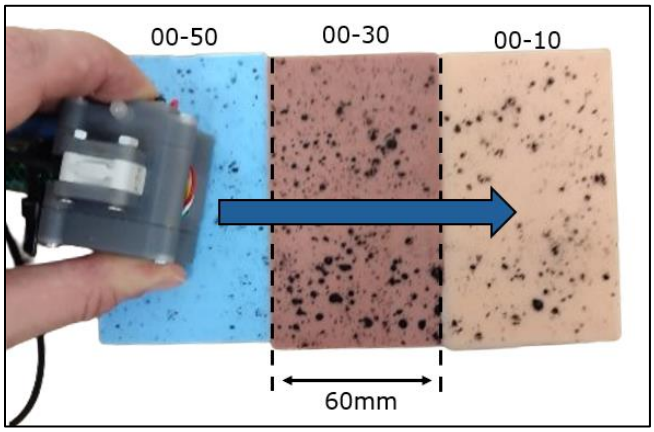

Fig. 11. Suction test setup.

The device, connected to a pump, was passed over the pads in order to lift the suction zone and measure the height and position of the acquired point. Analyzing the results, it is easy to observe that decreasing the hardness produces an increase in lift with a trend in line with the characteristics of the silicones chosen (Fig. 12).

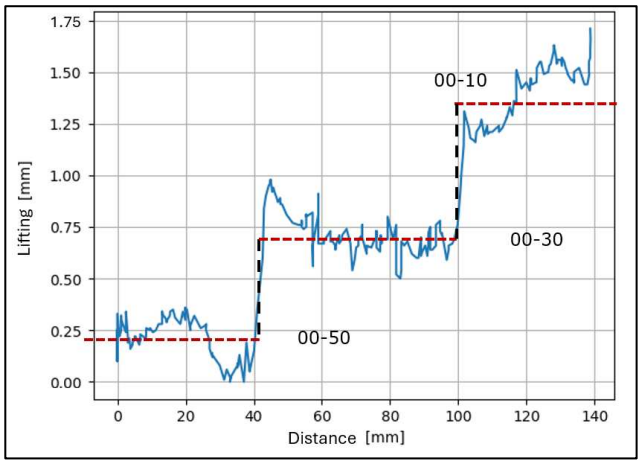

Fig. 12. graph of lift as a function of distance travelled. it can be observed that there is a clear difference in lift as the material varies.

VI. Conclusions

This study proposes a new approach to objectively assess the pliability of burn scars in pediatric cases by redesigning the LPG-D probe with the incorporation of a position detection system based on magnetic encoders. Tests conducted have shown that the device is accurate and reliable, offering an objective assessment of scar pliability. This new approach could significantly improve the management of burn scar treatments in pediatric patients, allowing for a more accurate assessment of treatment efficacy.

To further improve the efficacy of this device, a possible improvement involves implementing a system to relocate the same acquisition position between therapeutic sessions. Although it is feasible to find references based on skin texture or natural landmarks of the patient during close sessions, it should be considered that in pediatric cases with extended treatment periods, changes in the patient's physiognomy may occur, rendering physical feature-based references unreliable. Additionally, a supplementary upgrade could involve replacing the wiring with wireless or Bluetooth communications to facilitate device use during treatment.

This study thus provides a solid basis for the development of more advanced tools and methodologies for the objective assessment of burn scars in pediatric patients, helping to improve the quality of treatments and the overall clinical outcome for this vulnerable patient population.

VII. Bibliography

[1] P. Li *et al.*, "The recovery of post-burn hypertrophic scar in a monitored pressure therapy intervention programme and the timing of intervention," *Burns*, vol. 44, no. 6, pp. 1451–1467, Sep. 2018, doi: 10.1016/j.burns.2018.01.008.

[2] R. L. Sheridan, "Burns in children," in *Journal of Burn Care and Research*, Lippincott Williams and Wilkins, 2017, pp. e618–e624. doi: 10.1097/BCR.0000000000000536.

[3] P. Ault, A. Plaza, and J. Paratz, "Scar massage for hypertrophic burns scarring—A systematic review," *Burns*, vol. 44, no. 1. Elsevier Ltd, pp. 24–38, Feb. 01, 2018. doi: 10.1016/j.burns.2017.05.006.

[4] A. Schulz, I. Rothermund, R. Lefering, ; Paul, C. Fuchs, and J. Schiefer, "Long-term Scar Quality after Treatment of Standardized Partial-Thickness Skin Graft Donor Sites," 2018.

[5] C. M. Ryan, I. Parry, and R. Richard, "Functional outcomes following burn injury," in *Journal of Burn Care and Research*, Lippincott Williams and Wilkins, 2017, pp. e614–e617. doi: 10.1097/BCR.0000000000000537.

[6] N. Brusselaers, A. Pirayesh, H. Hoeksema, J. Verbelen, S. Blot, and S. Monstrey, "Burn scar assessment: A systematic review of different scar scales," *Journal of Surgical Research*, vol. 164, no. 1. Nov. 2010. doi: 10.1016/j.jss.2010.05.056.

[7] M. Bozkurt, F. Ceran, E. Guvercin, and G. T. Filinte, "A new method for scar tissue assessment: Modified POSAS observer scale," *Burns*, vol. 43, no. 2. Elsevier Ltd, pp. 445–448, Mar. 01, 2017. doi: 10.1016/j.burns.2016.04.022.

[8] G. V Oliveira, D. Chinkes, C. Mitchell, G. Oliveras, H. K. Hawkins, and D. N. Herndon, "Objective Assessment of Burn Scar Vascularity, Erythema, Pliability, Thickness, and Planimetry."

[9] D. M. Perry, D. A. McGrouther, and A. Bayat, "Current tools for noninvasive objective assessment of skin scars," *Plast Reconstr Surg*, vol. 126, no. 3, pp. 912–923, Sep. 2010, doi: 10.1097/PRS.0b013e3181e6046b.

[10] H. DeJong *et al.*, "A Novel, Reliable Protocol to Objectively Assess Scar Stiffness Using Shear Wave Elastography," *Ultrasound Med Biol*, vol. 46, no. 7, pp. 1614–1629, Jul. 2020, doi: 10.1016/j.ultrasmedbio.2020.03.003.

[11] K. C. Lee, J. Dretzke, L. Grover, A. Logan, and N. Moiemen, "A systematic review of objective burn scar measurements," *Burns and Trauma*, vol. 4, no. 1. Oxford University Press, Dec. 01, 2016. doi: 10.1186/s41038-016-0036-x.

[12] Z. Tyack, M. Simons, A. Spinks, and J. Wasiak, "A systematic review of the quality of burn scar rating scales for clinical and research use," *Burns*, vol. 38, no. 1. pp. 6–18, Feb. 2012. doi: 10.1016/j.burns.2011.09.021.

[13] D. Promny, M. Billner, and B. Reichert, "Objective burn depth assessment of hand burns," *Handchirurgie Mikrochirurgie Plastische Chirurgie*, vol. 51, no. 5, pp. 362–366, 2019, doi: 10.1055/a-0991-7869.

[14] C. M. Legemate *et al.*, "Evaluation of measurement properties of health-related quality of life instruments for burns: A systematic review," in *Journal of Trauma and Acute Care Surgery*, Lippincott Williams and Wilkins, Apr. 2020, pp. 555–571. doi: 10.1097/TA.0000000000002584.

[15] A. Moseley, N. Piller, J. Douglass, and M. Esplin, "Comparison of the effectiveness of MLD and LPG technique®," *J Lymphoedema*, vol. 2, no. 2, pp. 2–8, 2007, [Online]. Available: http://www.inanir.com/dosya/comparison-mld-lpg.pdf

[16] P. B. Fodor, "Endermologie (LPG): Does It Work ?" p. 1997, 1997.

[17] F. Dalle Mura, L. Governi, R. Furferi, M. Cervo, and L. Puggelli, "Towards the Development of a Device for Assessing the Pliability of Burn Scars," *Front Bioeng Biotechnol*, vol. 10, no. June, pp. 1–13, 2022, doi: 10.3389/fbioe.2022.856562.

[18] T. Feng, W. Chen, J. Qiu, and S. Hao, "A new kind of absolute magnetic encoder," *Sensors*, vol. 21, no. 9, 2021, doi: 10.3390/s21093095.

[19] ams OSRAM Group, "AS5600- Product Document," 2018. Accessed: Feb. 29, 2024. [Online]. Available: https://look.ams-osram.com/m/7059eac7531a86fd/original/AS5600-DS000365.pdf

[20] ATMEL - Enabling Unlimited Possibilities, "ATmega16U4/ATmega32U4, 8-bit Microcontroller with 16/32K bytes of ISP Flash and USB Controller - DATASHEET", Accessed: Jul. 01, 2015. [Online]. Available: https://dfimg.dfrobot.com/nobody/wiki/5397fcd9305ff620782aceb5d950ee84.pdf

[21] SensoPart Industriesensorik GmbH, "FT 10-RLA." Accessed: May 01, 2021. [Online]. Available: https://www.sensopart.com/index.php?eID=dumpFile&t=f&f=1002&token=3f93328f8a90b370b8a02821d85e884de9da76bb

[22] Smooth-On, "Dragon Skin™ Series - PRODUCT OVERVIEW." [Online]. Available: https://www.smooth-on.com/tb/files/DRAGON_SKIN_SERIES_TB.pdf

[23] Formlabs, "Grey Pro Form - Resin for Versatile Prototyping." [Online]. Available: https://formlabs-media.formlabs.com/datasheets/1801086-TDS-ENUS-0P.pdf

[24] Smooth-On, "Ecoflex™ Series - PRODUCT OVERVIEW", [Online]. Available: https://www.smooth-on.com/tb/files/ECOFLEX_SERIES_TB.pdf